

# Wide-field two-dimensional multifocal optical-resolution photoacoustic-computed microscopy

Jun Xia,<sup>1</sup> Guo Li,<sup>1</sup> Lidai Wang,<sup>1</sup> Mohammadreza Nasiriavanaki,<sup>1</sup> Konstantin Maslov,<sup>1</sup>  
John A. Engelbach,<sup>2</sup> Joel R. Garbow,<sup>2</sup> and Lihong V. Wang<sup>1,\*</sup>

<sup>1</sup>Department of Biomedical Engineering, Washington University in St. Louis, One Brookings Drive, St. Louis, Missouri 63130, USA

<sup>2</sup>Department of Radiology, Washington University in St. Louis, 660 S. Euclid Ave, St. Louis, Missouri 63110, USA

\*Corresponding author: [lhwang@wustl.edu](mailto:lhwang@wustl.edu)

Received October 7, 2013; revised November 2, 2013; accepted November 3, 2013;  
posted November 6, 2013 (Doc. ID 198591); published December 3, 2013

Optical-resolution photoacoustic microscopy (OR-PAM) is an emerging technique that directly images optical absorption in tissue at high spatial resolution. To date, the majority of OR-PAM systems are based on single-focused optical excitation and ultrasonic detection, limiting the wide-field imaging speed. While 1D multifocal OR-PAM (1D-MFOR-PAM) has been developed, the potential of microlens and transducer arrays has not been fully realized. Here we present the development of 2D multifocal optical-resolution photoacoustic-computed microscopy (2D-MFOR-PACM), using a 2D microlens array and a full-ring ultrasonic transducer array. The 10 mm × 10 mm microlens array generates 1800 optical foci within the focal plane of the 512-element transducer array, and raster scanning the microlens array yields optical-resolution photoacoustic images. The system has improved the in-plane resolution of a full-ring transducer array from  $\geq 100$  to 29  $\mu\text{m}$  and achieved an imaging time of 36 s over a 10 mm × 10 mm field of view. In comparison, the 1D-MFOR-PAM would take more than 4 min to image over the same field of view. The imaging capability of the system was demonstrated on phantoms and animals both *ex vivo* and *in vivo*. © 2013 Optical Society of America

OCIS codes: (110.0180) Microscopy; (110.5120) Photoacoustic imaging; (170.7170) Ultrasound; (110.5125) Photoacoustics.

<http://dx.doi.org/10.1364/OL.38.005236>

With its unique advantage of directly imaging optical absorption in tissue at a high spatial resolution, optical-resolution photoacoustic microscopy (OR-PAM) has found broad applications in biomedical research. To date, the majority of OR-PAM systems are based on a single optical focus and a single-element ultrasonic transducer. Therefore, high-speed imaging over a large field of view is challenging. To improve the imaging speed, fast scanning mechanisms and high-repetition-rate lasers have been utilized [1]; however, high-speed lasers usually lack wavelength tunability, limiting the scope of applications. Alternatively, multiple optical foci can be formed from a low-repetition-rate tunable laser for parallel detection. To this end, multifocal OR-PAM (MFOR-PAM) has been developed utilizing a microlens array to generate a 1D array of optical foci. The corresponding photoacoustic signals were detected using a linear transducer array [2]. While promising images have been acquired, MFOR-PAM has not fully exploited the potential of microlens and transducer arrays. Both arrays can be extended from 1D to 2D. Due to difficulties in confocal alignment, the current MFOR-PAM mechanically scans the sample, instead of the microlens and transducer arrays, making the system inconvenient for practical applications. Moreover, in an effort to achieve coaxial optical excitation and acoustic detection in reflection mode, a small portion of the transducer array is blocked by the microlens array, degrading the detection sensitivity [3].

In this Letter, we introduce a 2D MFOR-PACM system, which employs a 2D microlens array for optical excitation and a full-ring transducer array [4] for acoustic detection. The term “computed microscopy” is utilized as each transducer element is unfocused in the detection plane, and image reconstruction is required. The 2D microlens array

generates thousands of optical foci within the acoustic focal plane, and raster scanning the microlens array generates optical resolution photoacoustic images. In comparison, the 1D-MFOR-PAM uses only 20 optical foci [3]. 2D-MFOR-PACM is also the first OR-PAM system with the optical focal axis orthogonal to the acoustic detection axis. This novel design eliminates the need for an optical-acoustic combiner and thereby improves the detection sensitivity. The performance of the system is demonstrated through imaging a leaf phantom, a maternal mouse uterus, and a mouse brain.

Figure 1 shows a 3D drawing of the 2D-MFOR-PACM system. An optical parametric oscillator (OPO) laser (basiScan OPO, Newport), pumped by a Nd:YAG laser (Brilliant B, Quantel), was used as the excitation source.

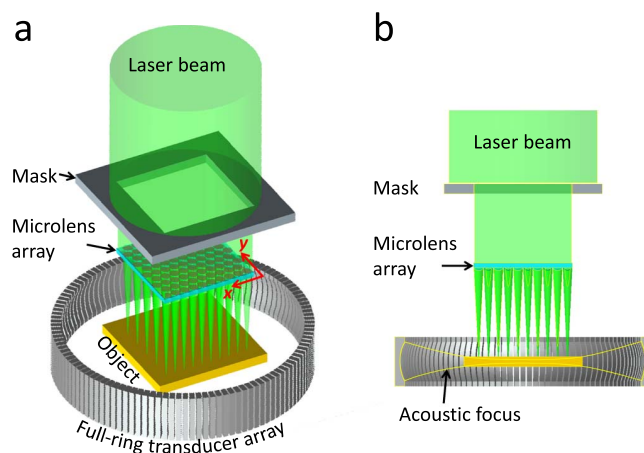


Fig. 1. Schematic drawing of the 2D-MFOR-PACM system. (a) 3D view of the system. (b) Cross-sectional view, especially highlighting the acoustic focus.

The laser has a pulse repetition rate of 10 Hz, an average output of 12 mJ per pulse, and a beam diameter of 16 mm. A 532 nm wavelength was used in all the experiments. To generate multiple optical foci, we used a 10 mm  $\times$  10 mm microlens array (18-00082, SUSS MicroOptics) consisting of a 40  $\times$  45 hexagonal grid of spherical microlens with 250  $\mu$ m center-to-center spacing. Each microlens has a diameter of a few micrometers less than 250  $\mu$ m and a radius of curvature of 835  $\mu$ m. Based on Zemax (Radiant Zemax LLC) simulation, the water-immersed microlens produces a diffraction-limited focus at 5.26 mm, with a focal diameter of 21.6  $\mu$ m at the waist. To avoid illuminating regions outside the lens, a mask with a 10 mm  $\times$  10 mm hole in the center was placed on top of the microlens array (Fig. 1). During the experiment, the two were raster-scanned concurrently along the  $x$  and  $y$  directions. For future quantitative imaging studies, the fluctuation in power distribution can be measured and calibrated by splitting a small portion of the masked beam to a beam profiler.

The photoacoustic signals are detected by a 512-element full-ring transducer array (Imasonic, Inc.) with a 5-MHz central frequency and greater than 80% reception bandwidth [4]. Each element in the array is arc-shaped in elevation to produce a focus at 19.8 mm. The combined foci of all elements generate a central focal region of 20 mm in diameter. The elevational thickness of the acoustic focal plane is approximately 1 mm, which is within the optical diffusion limit and is smaller than the depth of focus (1.38 mm) of the microlens array. The photoacoustic signals are digitized by a 64-channel data-acquisition (DAQ) system with a 40 MHz sampling rate. Due to the limited data-transfer speed, the DAQ can only acquire signals from every other laser pulse, yielding a full-ring acquisition time of 1.6 (0.2  $\times$  8) s.

To quantify the spatial resolution of the 2D-MFOR-PACM system, we used 6  $\mu$ m diameter carbon fiber fixed on top of an agar gel. The microlens was scanned across the carbon fiber in 1D at 2.27  $\mu$ m per step. We then reconstructed a PACT image at each scanning step and identified a pixel corresponding to the center of the carbon fiber. We then plotted the signal intensity of that pixel over different scanning steps to get the line-spread function [Fig. 2(a)]. The FWHM of the line-spread function is estimated to be 29.4  $\mu$ m, which is larger than the theoretical focal diameter of 21.6  $\mu$ m. This is possibly due to the low beam quality of the OPO laser, in addition to the finite size of the carbon-fiber target. We estimated the

optical fluence at the focus in water to be 443 mJ/cm<sup>2</sup>, which is 10 times lower than the damage threshold for red blood cells [5]. It should be noted that, depending on the depth of the focal point, the surface fluence that ANSI regulates [6] is much lower than this peak value.

Without the microlens array, the system is a conventional photoacoustic computed tomography (PACT) setup, with acoustically defined spatial resolution. Figure 2(b) compares the spatial resolution of the PACT and 2D-MFOR-PACM systems. The spatial resolution at other positions was derived theoretically [7] based on measurement results at the ring center, where the acoustic spatial resolution is the highest. As expected, the optical focus improves the spatial resolution by more than three times, from  $\geq 100$  to 29  $\mu$ m. It should also be noted that both the radial and tangential acoustic resolutions are much smaller than the pitch of the microlens (250  $\mu$ m), allowing signals from adjacent optical foci to be acoustically separated.

In phantom and animal experiments, the microlens array was raster scanned with a 25  $\mu$ m step size, yielding 90 steps (9  $\times$  10, due to the hexagonal grid, the microlens array has denser elements along one axis than the other) for a complete scan. Because each transducer element is unfocused in the imaging plane, 2D-MFOR-PACM requires image reconstruction. For each scanning step, we reconstruct a PACT image using back-projection. Within each 25  $\mu$ m optical focus in the PACT image, we identify the maximum amplitude and set all pixels to that maximum. We then zero-out all pixels outside the optical foci. The resulting image is a partial optical-resolution image for the given scanning step. The 2D-MFOR-PACM image can then be obtained by summing partial optical-resolution images of all scanning steps. To illustrate the reconstruction procedure, Media 1 is used to show the back-projected image at each scanning step and the summed partial optical-resolution image up to the given scanning step. An important part of reconstruction is to identify the absolute coordinates of the initial optical foci in the lab coordinate system. Because the pattern of microlens is already known in its local coordinate system, we create a matrix of the same size as the reconstructed image. In this matrix, the points within the 25  $\mu$ m optical foci are set to unity, and the points outside the optical foci are set to zero. We then shift the matrix along the  $x$  and  $y$  directions to find a position that yields the maximum cross-correlation coefficient with the PACT image. The optical foci for the following scanning steps can be localized by simply shifting the original matrix according to the scanning direction and distance.

To test the performance of the system, we first imaged a skeleton leaf, which contains a rich network of vessels with different diameters. Figure 3 shows the imaging results. The conventional PACT image was obtained by summing the back-projection images from all scanning steps directly. The resulting image is equivalent to the one obtained from planar light illumination. This reconstruction procedure ensures the conventional and optical-resolution photoacoustic images to have identical optical illumination profiles and total delivered laser energy. In Fig. 3(a), we can see that the vessels are blurred due to the worse acoustic resolution. In contrast, the

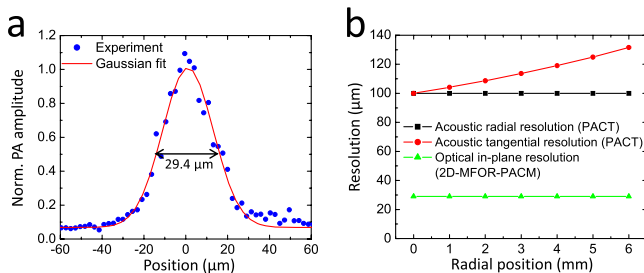


Fig. 2. In-plane resolution of the 2D-MFOR-PACM system. (a) Line-spread function used to measure the in-plane resolution of the 2D-MFOR-PACM system. (b) Comparison of spatial resolutions of PACT and 2D-MFOR-PACM systems.

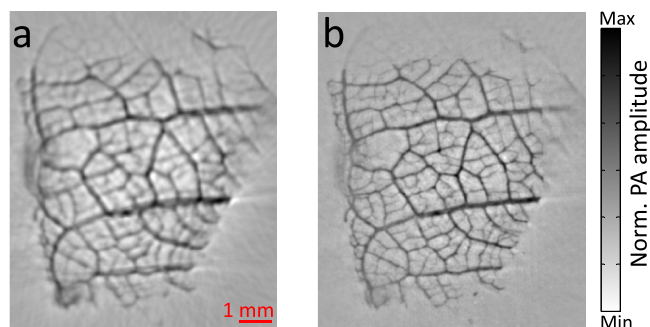


Fig. 3. Experimental results of a skeleton leaf phantom. (a) Conventional PACT image. (b) 2D-MFOR-PACM image. (Media 1).

2D-MFOR-PACM image shows detailed vascular structures at a high optical resolution.

We further tested the system by imaging blood vessels in a maternal mouse uterus. The uterine blood vessels provide oxygen and nutrients to the embryo *via* the placenta and are essential for normal fetal development [8]. The uterus was excised from a euthanized pregnant mouse on gestation day 14.5. After extraction, the uterine artery was sealed using glue to preserve the blood. The sample was then mounted on the imaging system, with one of two placentas present within the uterus facing the lower portion of the imaging region. Figure 4 compares the conventional PACT and 2D-MFOR-PACM images. As expected, the 2D-MFOR-PACM image shows a higher spatial resolution and allows clear identification of small blood vessels. Due to the small diameter of the transducer array, the experiment was performed *ex vivo*. With a larger transducer array, the maternal uterus could be imaged *in vivo*. Combined with ring-shaped light illumination for noninvasive whole-body imaging [9,10], the full-ring array system can potentially provide multiscale imaging for maternal-fetal research.

Finally, we demonstrated the *in vivo* imaging capability of the system by imaging a mouse brain. A two-month-old Swiss Webster mouse was anesthetized with isoflurane and mounted on a lab-made animal holder.

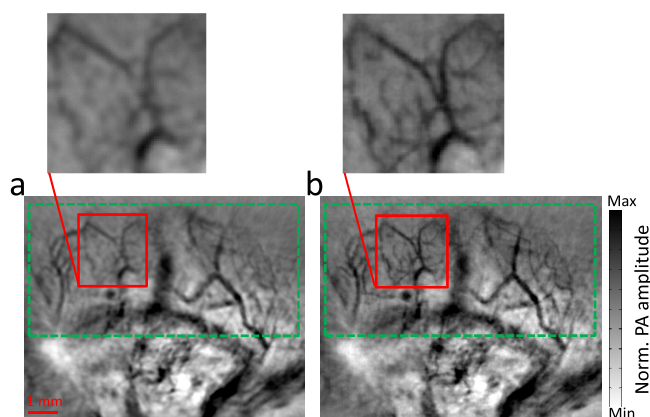


Fig. 4. *Ex vivo* images of an intact uterus from a pregnant mouse on gestation day 14.5. The lower portions of these images show one of two placentas present in this mouse. (a) Conventional PACT image. (b) 2D-MFOR-PACM image. (Media 2 (4.0 MB) highlights the regions within the green dashed line.

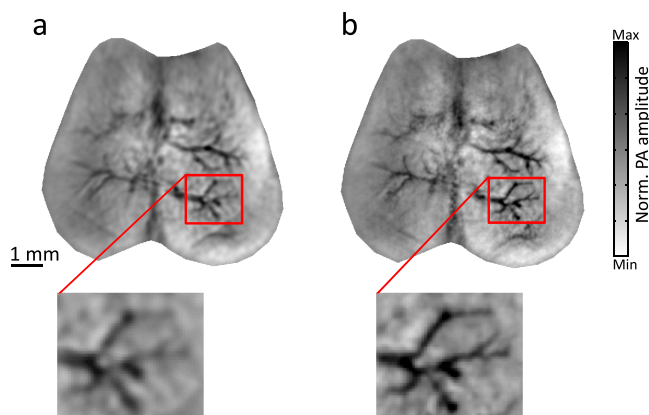


Fig. 5. *In vivo* images of cortical vasculature in a mouse brain. (a) Conventional PACT image. (b) 2D-MFOR-PACM image. (Media 3, 3.0 MB).

To allow optical focusing on the cortex, the scalp was removed before the experiment. For imaging at high spatial resolution, it is essential to mitigate any motions. Therefore, we installed two ear bars and a tooth bar on the holder for stabilization of the head. During the experiment, the animal was mounted underneath the water tank, and the brain was imaged through a flexible membrane. A detailed description of the animal-mounting procedure can be found in [9,11]. Figure 5(a) shows conventional PACT images of the cortical vasculature. From the enlarged image, we can clearly see that the vessels are blurred due to the acoustic resolution. In contrast, the 2D-MFOR-PACM image shows sharp vascular structures. Comparison between the two images also can be found in Media 3.

To demonstrate the best images accessible using the system, all of the above images were acquired with 512-element acquisition at each scanning step, yielding 144 s ( $1.6 \times 90$ ) for a 2D-MFOR-PACM scan. The field of view ( $10 \text{ mm} \times 10 \text{ mm}$ ) of the current system is limited only by the size of the microlens array. Using a larger microlens array, the system can image a larger region within the same amount of time. The imaging speed can be further improved based on sparse sampling of the full-ring array, i.e., acquire data from a fewer number of elements at each scanning step. Images of 64 elements per step, 128 elements per step, and 256 elements per step scans are shown in Fig. 6. To quantitatively evaluate the image quality, we calculated the structural similarity (SSIM) index [12] between the images in Fig. 6 and the reference image [Fig. 3(b)]. The SSIM index has been chosen because it matches well to the perceived visual

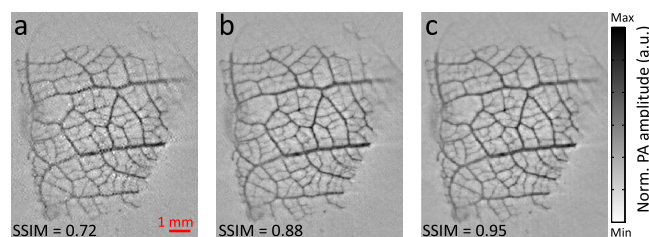


Fig. 6. 2D-MFOR-PACM images reconstructed from (a) 64 elements per step, (b) 128 elements per step, and (c) 256 elements per step scans.

quality, and an SSIM index of one means that the two images are visually identical. The results are written in the bottom left corner of each image. It can be seen that the 128- and 256-element indexes are comparable, and both are much higher than that of the 64-element image. Therefore the scanning time can be shortened to 36 s without visually compromising the image quality. The 64-element image [Fig. 5(a)] contains some artifacts. However, it still reveals small vascular structures that can hardly be seen in the conventional PACT image [Fig. 3(a)].

The image artifacts in Fig. 5(a) are caused by the transducer array's channel map, in which the 64 elements in a single acquisition are not evenly distributed around the full ring and are leaving more than 50% of the aperture uncovered [13]. The 128 and 256 elements, from two and four acquisitions, respectively, are evenly distributed around the full ring and hence provide better images. With advanced image-reconstruction algorithms or an optimized channel map, we expect the 64-element image to be further improved, shortening the scanning time to 18 s. In comparison, the 1D-MFOR-PAM system in [3] needs 150 s to image over a 5 mm × 6 mm region. Other high-speed OR-PAM systems have an even smaller field of view and require partitioning a large object into multiple smaller regions [1]. However, translating the sample and realigning the system may take several minutes.

In summary, a new OR-PAM system, 2D-MFOR-PACM, has been developed based on 2D multifocal optical excitation and full-ring transducer array detection. The imaging capability of the system was demonstrated through phantom and animal experiments. To avoid acoustic reflection, we opted to use a microlens array with a long focal length, rendering a relatively low numerical aperture (NA). If the acoustic reflection can be properly accounted for, we can employ a high NA microlens array to improve the system's spatial resolution further. The principle of 2D-MFOR-PACM also can be applied to other cross-sectional PACT systems, allowing multiscale imaging. The current imaging speed is mainly limited by the DAQ system, which operates at 5 Hz. With a high-repetition-rate laser and a matched DAQ system, the imaging time can be shortened to less than 0.05 s, reaching video rate. Mechanical scanning of the microlens array also can be replaced by optical mirror steering of the excitation beam, allowing high-speed 2D scanning. Moreover, without sacrificing speed, the imaging region can be enlarged up to the size of the microlens array or the field-of-view of the transducer array. Besides the

improvement in imaging speed, 2D-MFOR-PACM also has higher detection sensitivity. This is because the total detection area in the full-ring transducer array is much larger than that of transducers used in conventional OR-PAM systems. With high scanning speed, wide scanning range, and high detection sensitivity, 2D-MFOR-PACM will find broad applications in biomedical research.

The authors appreciate Prof. Sandra Matteucci's careful reading of the manuscript. This work was sponsored, in part, by National Institutes of Health grants DP1 EB016986 (NIH Director's Pioneer Award), R01 EB016963, R01 EB008085, R01 CA134539, U54 CA136398, R01 CA157277, and R01 CA159959 and by the United States-Israel Binational Science Foundation grant 2011405 (J. R. G.). L. W. has a financial interest in Microphotoacoustics, Inc., and Endra, Inc., which, however, did not support this work. K. M. has a financial interest in Microphotoacoustics, Inc., which, however, did not support this work.

## References

1. J. Yao and L. V. Wang, *Laser Photon. Rev.* **7**, 758 (2013).
2. L. Song, K. Maslov, and L. V. Wang, *Opt. Lett.* **36**, 1236 (2011).
3. G. Li, K. I. Maslov, and L. V. Wang, *J. Biomed. Opt.* **18**, 030501 (2013).
4. J. Gamelin, A. Maurudis, A. Aguirre, F. Huang, P. Guo, L. V. Wang, and Q. Zhu, *Opt. Express* **17**, 10489 (2009).
5. D. O. Lapotko and E. Y. Lukianova, *Lasers Surg. Med.* **36**, 13 (2005).
6. Laser Institute of America, *American National Standard for the Safe Use of Lasers* (American National Standard Institute, 2000).
7. M. Xu, in *Photoacoustic Imaging and Spectroscopy* (CRC Press, 2009), pp. 47–60.
8. Z. Madeja, H. Yadi, R. Apps, S. Boulenouar, S. J. Roper, L. Gardner, A. Moffett, F. Colucci, and M. Hemberger, *Proc. Natl. Acad. Sci. USA* **108**, 4012 (2011).
9. J. Xia, M. Chatni, K. Maslov, Z. Guo, K. Wang, M. Anastasio, and L. V. Wang, *J. Biomed. Opt.* **17**, 050506 (2012).
10. M. R. Chatni, J. Xia, R. Sohn, K. Maslov, Z. Guo, Y. Zhang, K. Wang, Y. Xia, M. Anastasio, J. Arbeit, and L. V. Wang, *J. Biomed. Opt.* **17**, 076012 (2012).
11. C. Li, A. Aguirre, J. Gamelin, A. Maurudis, Q. Zhu, and L. V. Wang, *J. Biomed. Opt.* **5**, 010509 (2010).
12. Z. Wang, A. C. Bovik, H. R. Sheikh, and E. P. Simoncelli, *IEEE Trans. Image Process.* **13**, 600 (2004).
13. J. K. Gamelin, A. Aguirre, and Q. Zhu, *Med. Phys.* **38**, 1503 (2011).